Hexagonally Perforated Lamella-to-Cylinder Transition in a Diblock Copolymer Thin Film under an Electric Field

Dung Q. Ly,[†,⊥] Takashi Honda,[‡] Toshihiro Kawakatsu,[§] and Andrei V. Zvelindovsky*[,†]

Centre for Materials Science, Department of Physics, Astronomy and Mathematics, University of Central Lancashire, Preston, PR1 2HE, United Kingdom; ZEON Corporation, 1-6-2, Marunouchi, Chioda-ku, Tokyo 100-8246, Japan; and Department of Physics, Tohoku University, Aoba, Aramaki, Aoba-ku, Sendai 980-8578, Japan

Received April 16, 2007; Revised Manuscript Received April 23, 2008

ABSTRACT: Using self-consistent-field simulation, a perforated lamella (PL) is investigated under an applied electric field. The perforated lamella is obtained by confining a cylinder-forming diblock copolymer melt in a thin film with a thickness of the spacing between cylinders in the bulk equilibrium state. Upon application of an electric field, the perforated lamella transforms to laying or standing cylinders depending on the direction of the electric field.

Block copolymers can microphase separate into various nanostructures. Typical nanostructures of a diblock copolymer in bulk are lamellar, cylindrical, gyroid, and spherical, depending on the volume fraction of individual blocks and the value of χN, where χ is the Flory−Huggins interaction parameter and N is the total number of statistical segments (each segment can contain a few monomer units).[1,2] Transition between different structures can be induced either by changing the temperature[3] or by applying external fields like a shear flow[4,5] or an electric field.[6,7]

Even for bulk systems without imposed external fields the dynamics of order−order transitions remains a very active research topic.[8] Understanding the effect of confinement on the block copolymers is much more limited.[9,10] In thin films, the microdomain structure has to adjust to the certain film thickness, which can be a noninteger multiple of the microdomain spacing in the bulk. For instance, depending on the film thickness and the strength of the surface interaction, a variety of phases were observed, namely, wetting layers, lamellae, perforated lamellae (PL), and parallel and perpendicular cylinders. These structures can be observed for various block copolymers which form cylindrical domains in the bulk.[11−14]

In the presence of an external electric field the phase behavior becomes very rich. Theoretical work on block copolymers under electric field has a long history.[6,7] Some of the first works in this field were on lamellar systems using the Landau−Ginzburg treatment[15,16] and lamellae and cylinders using the strong segregation approach.[17] The underlying dielectric mechanism was proposed earlier in refs 18–20. The first application of self-consistent-field theory (SCFT) to the problem was done in our work[21] which used a dynamic version of SCFT. Later we applied that treatment to all classical phases (lamellae, cylinders, spheres).[22−30] Consequently, several other groups studied these classical phases using static SCFT.[31−37] Although the dynamic SCFT allows for studying the kinetics of phase transitions,[29] the static SCFT includes more complete treatment of the electrostatic energy.[31,34] Recently, we complemented our study of spherical phase by a dynamic Landau−Ginzburg approach.[38] To summarize the behavior of these systems, sphere-forming systems respond to an applied electric field by elongating spheres in the direction of the electric field.[6] For lamella- and cylinder-forming systems, domains are reoriented in the direction of the applied electric field.[6,7] The remaining stable bulk phase, which was not studied, is a complex phase gyroid. Very recently, we presented studies of gyroid-to-cylinder transition under an electric field in the bulk using both dynamic SCFT and dynamic Landau−Ginzburg approach.[39,40]

The phase behavior in thin films is much different. The perforated lamella (PL) phase, which is metastable in the bulk, can be stabilized in thin films as a surface reconstruction.[12] PL phase is believed to be a promising candidate to create complex structures in soft nanotechnology using thin films of block copolymers.[13] The PL phase is a natural candidate to create ordered nanoporous polymer films, the topic of long-lasting interest due to its applications in size-selective catalyst supports and advanced separations.[41] To tailor a desired structure, a manipulation by external field can be used. For that reason a complete understanding of possible transitions involving PL phase is very much desired. These transitions can be very nontrivial even without any externally imposed fields.[14] This was the motivation of our present study of a hexagonally perforated lamella, a structure, which is normally not stable in the bulk. Here, PL is confined between a pair of parallel walls and is subjected to an applied electric field. PL phase under electric fields has not yet been studied experimentally.

We study an A−B diblock copolymer melt, with each polymer chain consisting of N_A segments of A-type and N_B segments of B-type. Therefore, the total number of statistical segments is $N = N_A + N_B$. The statistical unit can be arbitrary as long as the size of the segment is larger than the persistent length. Our goal is to study how the morphology transforms in time under an applied electric field. For this purpose we use a dynamic version of SCFT.[39,42−46] For the dynamic model, we use a Fick's law of linear diffusion dynamics where the flux of the segments is proportional to the local gradient of the chemical potential.[39] This assumption of linear diffusion is valid when the characteristic relaxation time of the chain conformation (Rouse time or reptation time) is faster than the characteristic time scale of the change in the segment distribution.[44,47] Under this assumption, we can use the static SCF theory to evaluate the free energy of the chain system by assuming that the chain conformation is always in equilibrium under the given segment density distribution.[44] These assumptions are essentially important in performing large-scale simulations because a large

* Corresponding author.
† University of Central Lancashire.
‡ ZEON Corporation.
§ Tohoku University.
⊥ Present address: AMEE, Brunel University, Uxbridge, London, UK.

10.1021/ma0708850 CCC: $40.75
Published on Web 05/30/2008

system size is required when we focus on the morphology transition.

When a dc electric field is applied, the dynamics has the form of an anisotropic diffusion, as was described in ref 22

$$\frac{\partial}{\partial t}\phi_K(\mathbf{r},t) = L_K\nabla^2\mu_K(\mathbf{r}) + \alpha\frac{\partial^2}{\partial n^2}\phi_K(\mathbf{r},t) \quad (1)$$

where the electric field is along the n-direction ($n = x$, y, or z in our simulation); ϕ_K is the local volume fraction of blocks of K-type (K = A or B). We assume that the system is incompressible. In the case of segments of the same volume, the average volume fraction of the A-block is $f = N_A/N$. The mobility L_K is taken the same for all components, $L_K = L$. The electric field of amplitude E_0 enters the dynamics in eq 1 via the parameter $\alpha = g_e v L$, where $g_e = \epsilon_1^2 E_0^2/(4\pi\bar{\epsilon})$ (CGS),[15] v is the volume of a single polymer chain, $\bar{\epsilon} = \epsilon|_{\phi_A} = f$ and $\epsilon_1 = (\partial\epsilon/\partial\phi_A)|_{\phi_A} = f$, with $\epsilon(\phi_A)$ being the dielectric constant of a nonuniform system with the composition ϕ_A.[22,29,39] Derivation of the last term in eq 1 follows straightforwardly from eq 10.18 in ref 48 (see refs 22 and 29 for details). We can introduce a dimensionless parameter:[22,29,39]

$$\tilde{\alpha} = \frac{\alpha}{kTL} = \frac{1}{4\pi}\frac{(\epsilon_A - \epsilon_B)^2}{\epsilon_A f + \epsilon_B(1-f)}\frac{E_0^2 v}{kT} \quad (2)$$

where k is Boltzmann constant, T is the temperature, and ϵ_K is the dielectric constant of pure K-block. We refer readers to ref 29, section II, which contains a comprehensive discussion of the parameter $\tilde{\alpha}$, defined by eq 2. It is worth noting that eq 1 is also valid for slowly varying ac electric fields (so that the time scale of the change in the electric field is large compared to the relaxation times of the polymer chain conformations). On the other hand, if the frequency of the ac electric field is much higher than the inverse of the relaxation time of the chain conformation, we cannot assume that the chain conformation is in equilibrium. In this case, we should take the effects of the nonequilibrium chain conformation due to the applied electric field or the entanglements between chains into account.[49–51] The chemical potential of blocks of K-type is defined as $\mu_K = \delta F/\delta\phi_K$, where F is the free energy of the system:[43,44,46]

$$F/kT = -M\ln Z - \sum_K \int d\mathbf{r}\, V_K(\mathbf{r})\,\phi_K(\mathbf{r}) + \frac{1}{2}\sum_K\sum_{K'}\int d\mathbf{r}\,\chi_{KK'}\phi_K(\mathbf{r})\,\phi_{K'}(\mathbf{r}) + \sum_K\int d\mathbf{r}\,\chi_{KW}\,\phi_K(\mathbf{r})\,\delta(\mathbf{r}-\mathbf{R}) \quad (3)$$

The first term in eq 3 includes the conformational entropy of chains, where M and Z are number of chains in the system and the partition function of a single block polymer chain, respectively. In the SCFT simulation, Z is evaluated by using a path integral calculation on the chain conformation. The second term in eq 3 is the contribution from the self-consistent potential $V_K(\mathbf{r})$. The third term is the interaction between segments, where $\chi_{KK'}$ is the interaction parameter between polymer segments of types K and K'. The fourth term is the interaction between segments and the surfaces of the walls, where the surfaces are treated as hard walls (W), whose position $\mathbf{R}$ is specified by the Dirac delta-function $\delta(\mathbf{r}-\mathbf{R})$. The interaction of polymer blocks with the wall is treated in the traditional SCFT way using the χ_{KW} parameter. We refer to a standard textbook, ref 52 (p 156), for details. The relationship between these parameters and the ones used in experiments is a separate issue. One of the ways to establish such a relationship is by mapping SCFT results to specific experiments.[12]

For the purpose of this paper the OCTA code,[45,46] which we use to perform SCFT simulation, was modified to account for the dynamics described by eq 1.[39]

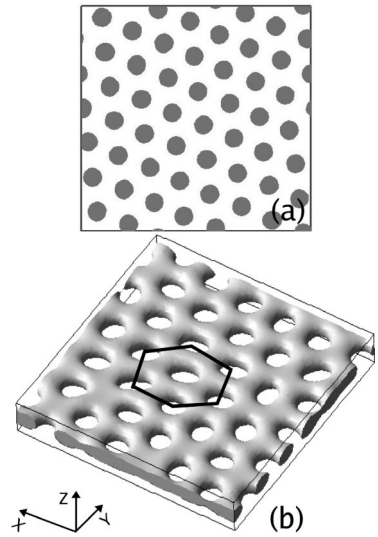

Figure 1. (a) 2D cylindrical structure of A_3B_6 copolymer melt obtained with a static SCFT calculation. The dark regions correspond to the A-phase. (b) Perforated lamellar structure at time $t = 100$. A hexagon is shown to guide the eye. Here and in all figures below the isosurface level is $\phi_A = 0.5$.

Bulk System. The parameters of our diblock copolymer melt are $N_A = 3$, $N_B = 6$ ($f = 0.33$); the Flory−Huggins interaction parameters $\chi_{AB} = 2$, and for simplicity we assume that $\chi_{AA} = \chi_{BB} = 0$ (see, e.g., ref 44, p 60). Because of the Gaussian nature of our chain model, the important parameter is $\chi_{AB}N$.[53] The values of χ_{AB} and N can be chosen arbitrarily as long as the product is the same. We refer the reader to an extensive discussion of the issue in ref 42. Choosing large N, we consider a system with negligible role of the thermal fluctuations for a given $\chi_{AB}N$.[54] In our work the parameter $\chi_{AB}N$ is equal to 18. This value corresponds to the hexagonally packed cylinders in the bulk. We have confirmed this by a 3D static SCFT simulation in a small box (not shown here). In order to accurately determine the equilibrium distance between cylindrical domains, a large box with defect-free cylinders is required. In the case of cylinders a static SCFT simulation in 2D is sufficient as well as the fastest and therefore is the most optimal.[45] Figure 1a shows the result in a simulation box of the size 32.0×32.0, with the spatial mesh width $\Delta x = \Delta y = 0.5$ (in units of segment size, that is taken to be unity). The mesh size along the chain, which is used in the calculation of the path integral, is $\Delta s = 0.2$. This 2D simulation mimics 3D bulk system. We measure that the distance between cylinders is about 4.5.

Perforated Lamella in Thin Film. The perforated lamellar phase can be induced by the presence of surfaces in a diblock copolymer melt for certain separation distances between the surfaces and strengths of surface−polymer segment interactions. The largest region of stability of PL phase is in films of thickness of one bulk interdomain spacing.[11] Therefore, we perform simulations in a simulation box with the size $32.0 \times 32.0 \times 4.5$ with surfaces modeled as parallel planes (walls), which are placed at $z = 0.0$ and $z = 4.5$. In the x- and y-directions (in-plane), the periodic boundary condition is used. The surface interaction is expressed as an effective interaction $\zeta = \chi_{AW} - \chi_{BW}$, where χ_{AW} and χ_{BW} are the interaction parameters between segment types A and B with the walls, respectively. For simplicity, we choose $\chi_{AW} = 0$. The perforated lamella in Figure 1b is obtained using the dynamic SCFT method with the following parameters: the interval time step used in integrating eq 1 $\Delta t = 0.001$, the mobility $L = 1$, and the surface interaction

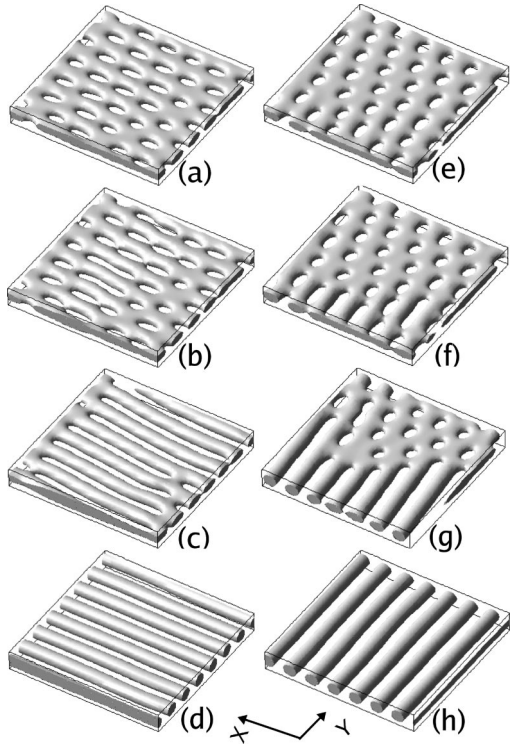

Figure 2. Kinetics of PL-to-cylinder transition under an in-plane electric field with $\tilde{\alpha} = 0.3$. Time: t = (a) 10, (b) 25, (c) 50, and (d) 400 for the electric field applied along x-direction and (e) 10, (f) 25, (g) 50, and (h) 400 for the electric field applied along y-direction.

$\zeta = 0.13$ (which means a preferential attraction of B-blocks to the walls).

Perforated Lamella under an Electric Field. First we consider the case with an applied field in-plane of the film (along x- or y-direction). If the electric field is weak, the system remains in the PL phase. If the electric field is above a certain threshold value, then we observe a transition to cylinders as is shown in Figure 2. In this case the arms of 3-fold connections that are not in the direction of the applied field break (Figure 2a,e). In the early stage of the transition we observe a formation of small patches of the undulating cylinders, and both PL and cylinders coexist (Figure 2b,c,f,g). These regions of undulating cylinders serve as nuclei, and the cylindrical phase develops by the nucleation and growth mechanism. At the end (Figure 2d,h) both systems transform to a cylindrical phase. The sequence of transient states is similar but reverse to the one observed for cylinder-to-PL transition under temperature or film thickness change.[14]

Next, we discuss the case of the electric field applied perpendicularly to the film plane (along the z-direction). The kinetic pathway of PL-to-cylinder transition is shown in Figure 3. The arms of the 3-fold connections that are perpendicular to the electric field break and gradually disappear, leaving the domains that are in the centers of these 3-fold connections to form standing cylinders. At $t = 200$, Figure 3e, we observe a cylindrical system with cylinders aligned parallel to the direction of the electric field. In this case the width of the cylinder is smaller in the vicinity of the wall compared to that of the middle of the cylinder (Figure 3f). This is because with $\zeta = 0.13$ the B-component is preferably attracted to the walls (or equivalently A-component is less preferred by the wall). Cylinders obtained for different electric field strengths are shown in Figure 4. From this figure we see that the cylinder obtained for a stronger field is less deviated from a perfect cylinder. This is because the contribution from the strong electric field which favors interfaces being parallel to the field dominates over the contribution from the interaction with the walls.

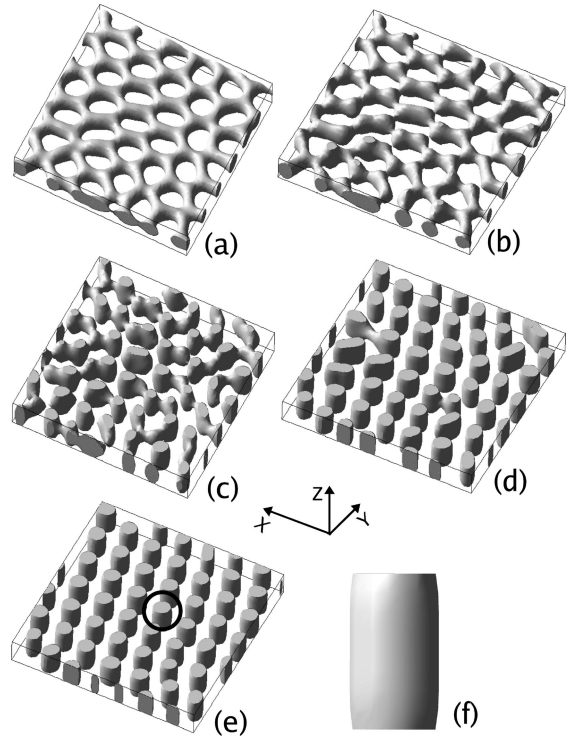

Figure 3. Kinetics of PL-to-cylinder transition under an electric field with $\tilde{\alpha} = 0.6$ applied in the z-direction. Time: (a) 1, (b) 3, (c) 5, (d) 10, and (e) 200. (f) A single cylinder extracted from (e), as indicated by a circle.

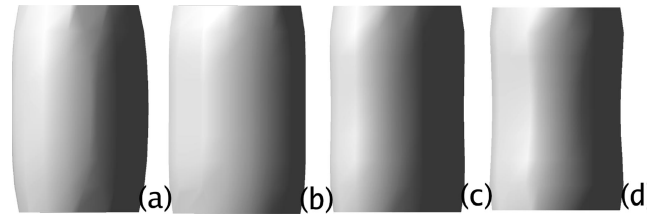

Figure 4. Different shapes of cylinders for different strengths of electric field $\tilde{\alpha}$: (a) 0.3, (b) 0.6, (c) 1.0, and (d) 2.0, with $\zeta = 0.13$.

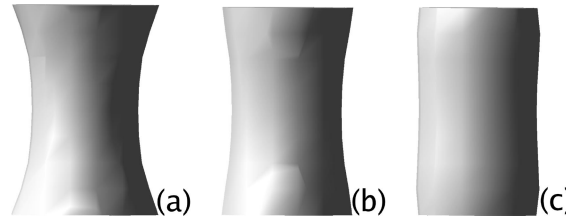

Figure 5. Different shapes of cylinders for different values of surface field ζ: (a) 0, (b) 0.05, and (c) 0.13, with $\tilde{\alpha} = 2.0$.

The phase transition from PL to cylinders for different surface field strengths is also calculated, as shown in Figure 5. For the cases of small values of ζ, i.e., $\zeta = 0.0$ and $\zeta = 0.05$, the cylinders have a bottleneck-like shape (Figure 5a,b), contrary to the case in Figure 4. The cylinders are wider in the vicinity of the walls, which can be explained as follows. Because the lengths of the subchains of A-type and that of B-type are different, it leads to different conformational entropic effects of the two domains (A and B). At $\zeta = 0$, the A-component (minority block) is preferred by the walls due to the entropic effects. As a result, in the vicinity of the walls we observe that the cylinders (A-component) are wider (Figure 5a). When the

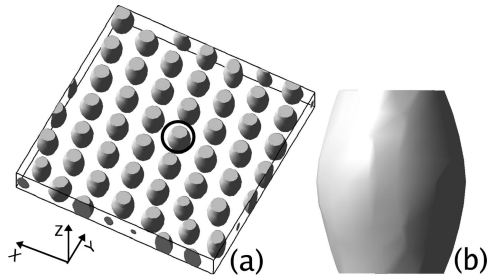

Figure 6. (a) Structure at $t = 100$ after the electric field was switched off from the structure in Figure 3e. (b) Single cylinder extracted from (a) as indicated by the circle.

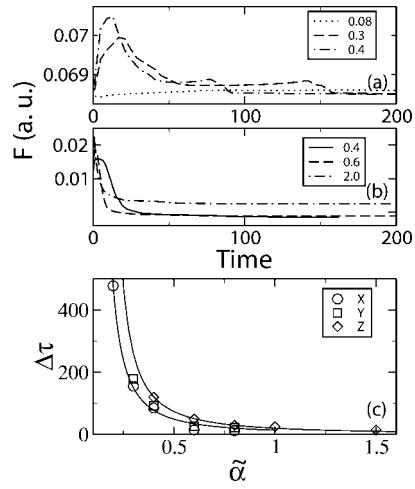

Figure 7. Free energy (in arbitrary units) as a function of time for different values of the applied field $\tilde{\alpha}$: (a) for x-direction and (b) for z-direction. (c) Transition time as a function of the electric field strength for x- (○), y- (□), and z- (◇) directions; solid lines are fits by the function $\Delta\tau \sim (\tilde{\alpha} - \tilde{\alpha}_0)^{-p}$.

value of ζ increases ($\zeta = 0.05$), the width of cylinders in the vicinity of the walls decreases as is shown in Figure 5b. For $\zeta = 0.13$ we obtain almost perfect cylinder (Figure 5c). This is because when ζ (or χ_{BW}) increases, the contribution from the interaction between B-components and the walls increases and neutralizes the entropic effect from the difference in block lengths.

When the electric field is switched off (starting from the structure in Figure 3e), the cylinders follow a kinetic pathway in the opposite direction: they become thicker in the middle of the film and narrower in the vicinity of the walls, as is shown in Figure 6. This is a pathway toward a PL phase as the cylinders will eventually joint each other in their middle parts. The process is rather slow, compared to PL-to-cylinders transition under electric field, indicating kinetic trapping of the structure.

Following our previous works,[29,39] we illustrate the transition using the free energy without electrostatic contribution, eq 3, which provides an insight into the change of the strength of microphase separation in time as well as changes in shapes and connectivity of domains. The applied electric field serves as a disturbance to the system, which manifests itself by a sharp increase in the free energy shortly after the electric field is applied at $t = 0$ (Figure 7a,b). In this initial stage the system changes the strength of its phase separation to some extent because the application of an electric field is similar to a shift in the temperature in the direction of the electric field.[39,55] If the electric field is weak ($\tilde{\alpha} = 0.08$, Figure 7a), the free energy reaches plateau and the system remains in the PL phase but with a slightly increased free energy. We call this state an "excited" state. If the field is above a certain threshold value, such an "excited" state has a finite lifetime. In such a case ($\tilde{\alpha} = 0.3$, Figure 7a), first the free energy sharply increases until $t = 10$ and then it decreases until $t = 60$ (first plateau). During this stage the system consists of both PL and cylinder phases (Figure 2a,b). From $t = 60$ to $t = 140$ we do not observe any change of the free energy. During this stage the system consists of cylinders with defects (Figure 2c). After $t = 140$ the free energy drops to another plateau, which corresponds to a defect-free cylindrical phase (Figure 2d). For all values of the electric field the second plateau is the same, which reflects the fact that the final cylindrical phase is the same for all fields. The stronger the applied field is, the faster the PL-to-cylinder transition occurs. We evaluate the lifetime $\Delta\tau$ of the "excited" state from the graphs in Figure 7a as the time span from the moment of the application of the electric field, $t = 0$, until the midpoint between the first and the second plateaus.[39] The values of the lifetime diverges as the strength of the electric field decreases. The result of fitting the data with $\Delta\tau \sim (\tilde{\alpha} - \tilde{\alpha}_0)^{-p}$ is shown in Figure 7c.

In the case of x- and y-directions the threshold value of the electric field is found to be $\tilde{\alpha}_0 = 0.11$ with the "critical" exponent $p = 1.55$. The transition processes in both cases are similar; however, the transition times are somewhat different. The difference becomes more noticeable for weaker electric fields. This can be attributed to the fact that x- and y-directions are not equivalent with respect to the orientation of the hexagonal pattern (see Figure 1b). It was shown (for the case of an applied shear) that different orientations of a structure with the hexagonal symmetry have different energies in an external field.[56] However, this effect is very weak.[56] This weak effect is easily suppressed by strong electric fields.

In the case of the electric field applied along z-direction, there are two features that are different from the cases of the lateral electric field. First, the free energy of the final cylinder phase is different for different values of the applied electric field. The weaker the applied field is, the lower the free energy becomes, as is shown in Figure 7b. Second, the threshold value of the applied field is larger compared to the case of lateral electric field. We obtain $\tilde{\alpha}_0 = 0.15$ with the "critical" exponent $p = 1.45$. The first difference is due to the fact that the final cylinders have different shapes (Figure 4). The second difference (different critical value of the electric field) can be attributed to the fact that the energy barrier, which separates PL and cylinder phase, is different in the case in Figure 3 compared to the case in Figure 2. This can be understood in terms of the symmetry change: the symmetries of the initial and the final structure in Figure 3 are very similar contrary to the case in Figure 2, where the starting and the final structure have different symmetries.

We note that a close value for the "critical" exponent ($p = 1.5$) is also found for the gyroid-to-cylinders transition under electric field both in dynamic SCFT and in cell dynamics simulation (for one of the transition pathways).[39,40]

In conclusion, by using the real-space dynamical SCFT, we investigate the cylinder forming diblock copolymer melt confined in a thin film. A hexagonally perforated lamella is obtained without an applied electric field. Under the electric field, the details of the kinetics of the transition, which includes intermediate structures, are studied. A threshold value of the applied electric field is required to induce the transition.

Acknowledgment. This work is partially supported by the national project on nanostructured polymeric materials, which has been entrusted to the Japan Chemical Innovation Institute by the New Energy and Industrial Technology Development Organization (NEDO) under METI's Program for the Scientific Technology Development for Industries that Creates New Industries. It is also supported by a grant-in-aid for science "Soft Matter Physics" from

the Ministry of Education, Culture, Sports, Science, and Technology, Japan. A.V.Z. acknowledges a short visit grant from The Royal Society (UK), which enabled him to visit T. Kawakatsu and T. Honda in Japan. All simulations were performed on SGI Altix 3700 at UCLan High Performance Computing Facilities in UK.

References and Notes

(1) *Nanostructured Soft Matter: Experiment, Theory, Simulation and Perspectives*; Zvelindovsky, A. V., Ed.; Springer: Dordrecht, 2007.
(2) Hamley, I. W. *The Physics of Block Copolymers*; Oxford University Press: Oxford, 1998.
(3) Wang, C. Y.; Lodge, T. P. *Macromolecules* **2002**, *35*, 6997.
(4) Zvelindovsky, A. V.; Sevink, G. J. A.; Fraaije, J. G. E. M. *Phys. Rev. E* **2000**, *62*, R3063.
(5) Honda, T.; Kawakatsu, T. *Macromolecules* **2006**, *39*, 2340.
(6) Xu, T.; Wang, J.; Russell, T. P. In *Nanostructured Soft Matter: Experiment, Theory, Simulation and Perspectives*; Springer: Dordrecht, 2007.
(7) Böker, A. In *Nanostructured Soft Matter: Experiment, Theory, Simulation and Perspectives*; Springer: Dordrecht, 2007.
(8) Yamada, K.; Komura, S. *J. Phys.: Condens. Matter* **2008**, *20*, 155107.
(9) Hashimoto, T.; Fukunaga, K. In *Nanostructured Soft Matter: Experiment, Theory, Simulation and Perspectives*; Springer: Dordrecht, 2007.
(10) Tsarkova, L. A. In *Nanostructured Soft Matter: Experiment, Theory, Simulation and Perspectives*; Springer: Dordrecht, 2007.
(11) Huinink, H. P.; Brokken-Zijp, J. C. M.; van Dijk, M. A.; Sevink, G. J. A. *J. Chem. Phys.* **2000**, *112*, 2452.
(12) Knoll, A.; Horvat, A.; Lyakhova, K. S.; Krausch, G.; Sevink, G. J. A.; Zvelindovsky, A. V.; Magerle, R. *Phys. Rev. Lett.* **2002**, *89*, 035501.
(13) Ludwigs, S.; Böker, A.; Voronov, A.; Rense, N.; Magerle, R.; Krausch, G. *Nat. Mater.* **2003**, *2*, 744.
(14) Knoll, A.; Lyakhova, K. S.; Horvat, A.; Krausch, G.; Sevink, G. J. A.; Zvelindovsky, A. V.; Magerle, R. *Nat. Mater.* **2004**, *3*, 886.
(15) Onuki, A.; Fukuda, J. *Macromolecules* **1995**, *28*, 8788.
(16) Tsori, Y.; Andelman, D. *Macromolecules* **2002**, *35*, 5161.
(17) Ashok, B.; Muthukumar, M.; Russell, T. P. *J. Chem. Phys.* **2001**, *115*, 1559.
(18) Amundson, K.; Helfand, E.; Davis, D. D.; Quan, X.; Patel, S. S.; Smith, S. D. *Macromolecules* **1991**, *24*, 6546.
(19) Amundson, K.; Helfand, E.; Quan, X.; Smith, S. D. *Macromolecules* **1993**, *26*, 2698.
(20) Amundson, K.; Helfand, E.; Quan, X.; Hudson, S. D.; Smith, S. D. *Macromolecules* **1994**, *27*, 6559.
(21) Kyrylyuk, A. V.; Zvelindovsky, A. V.; Sevink, G. J. A.; Fraaije, J. G. E. M. *Macromolecules* **2002**, *35*, 1473.
(22) Zvelindovsky, A. V.; Sevink, G. J. A. *Phys. Rev. Lett.* **2003**, *90*, 049601.
(23) Kyrylyuk, A. V.; Sevink, G. J. A.; Zvelindovsky, A. V.; Fraaije, J. G. E. M. *Macromol. Theory Simul.* **2003**, *12*, 508.
(24) Böker, A.; Elbs, H.; Hänsel, H.; Knoll, A.; Ludwigs, S.; Zettl, H.; Zvelindovsky, A. V.; Sevink, G. J. A.; Urban, V.; Abetz, V.; Müller, A. H. E.; Krausch, G. *Macromolecules* **2003**, *36*, 8078.
(25) Xu, T.; Zvelindovsky, A. V.; Sevink, G. J. A.; Gang, O.; Ocko, B.; Zhu, Y.; Gido, S. P.; Russell, T. P. *Macromolecules* **2004**, *37*, 6980.
(26) Zvelindovsky, A. V.; Sevink, G. J. A. *J. Chem. Phys.* **2005**, *123*, 074903.
(27) Xu, T.; Zvelindovsky, A. V.; Sevink, G. J. A.; Lyakhova, K. S.; Jinnai, H.; Russell, T. P. *Macromolecules* **2005**, *38*, 10788.
(28) Schmidt, K.; Böker, A.; Zettl, H.; Schubert, F.; Hänsel, H.; Fischer, F.; Weiss, T. M.; Abetz, V.; Zvelindovsky, A. V.; Sevink, G. J. A.; Krausch, G. *Langmuir* **2005**, *21*, 11974.
(29) Lyakhova, K. S.; Zvelindovsky, A. V.; Sevink, G. J. A. *Macromolecules* **2006**, *39*, 3024.
(30) Schmidt, K.; Schoberth, H. G.; Schubert, F.; Hänsel, H.; Fischer, F.; Weiss, T. M.; Sevink, G. J. A.; Zvelindovsky, A. V.; Böker, A.; Krausch, G. *Soft Matter* **2007**, *3*, 448.
(31) Lin, C.-Y.; Schick, M.; Andelman, D. *Macromolecules* **2005**, *38*, 5766.
(32) Lin, C.-Y.; Schick, M. *J. Chem. Phys.* **2006**, *125*, 034902.
(33) Matsen, M. W. *Phys. Rev. Lett.* **2005**, *95*, 258302.
(34) Matsen, M. W. *J. Chem. Phys.* **2006**, *125*, 074906.
(35) Tsori, Y.; Andelman, D.; Lin, C.-Y.; Schick, M. *Macromolecules* **2006**, *39*, 289.
(36) Matsen, M. W. *Macromolecules* **2006**, *39*, 5512.
(37) Matsen, M. W. *Soft Matter* **2006**, *2*, 1048.
(38) Pinna, M.; Zvelindovsky, A. V.; Todd, S.; Goldbeck-Wood, G. *J. Chem. Phys.* **2006**, *125*, 154905.
(39) Ly, D. Q.; Honda, T.; Kawakatsu, T.; Zvelindovsky, A. V. *Macromolecules* **2007**, *40*, 2928.
(40) Pinna, M.; Zvelindovsky, A. V. *Soft Matter* **2008**, *4*, 316.
(41) Zalusky, A. S.; Olayo-Valles, R.; Wolf, J. H.; Hillmyer, M. A. *J. Am. Chem. Soc.* **2002**, *124*, 12761.
(42) van Vlimmeren, B. A. C.; Maurits, N. M.; Zvelindovsky, A. V.; Sevink, G. J. A.; Fraaije, J. G. E. M. *Macromolecules* **1999**, *32*, 646.
(43) Sevink, G. J. A.; Zvelindovsky, A. V.; van Vlimmeren, B. A. C.; Maurits, N. M.; Fraaije, J. G. E. M. *J. Chem. Phys.* **1999**, *110*, 2250.
(44) Kawakatsu, T. *Statistical Physics of Polymers: An Introduction*; Springer: Berlin, 2004.
(45) Honda, T.; Kawakatsu, T. In *Nanostructured Soft Matter: Experiment, Theory, Simulation and Perspectives*; Springer; Dordrecht, 2007.
(46) Honda, T.; Kodama, H.; Roan, J.-R.; Morita, H.; Urashita, S.; Hasegawa, R.; Yokomizo, K.; Kawakatsu, T.; Doi, M. *SUSHI Users Manual*; OCTA: Nagoya, 2004 (http://octa.jp).
(47) Doi, M.; Edwards, S. F. *The Theory of Polymer Dynamics*; Oxford University Press: Oxford, 1986.
(48) Landau, L. D.; Lifshitz, E. M. *Electrodynamics of Continuous Media*; Pergamon Press: Oxford, 1960.
(49) Shima, T.; Kuni, H.; Okabe, Y.; Doi, M.; Yuan, X.-F.; Kawakatsu, T. *Macromolecues* **2003**, *36*, 9199.
(50) Mihajlovic, M.; Lo, T. S.; Shnidman, Y. *Phys. Rev. E* **2005**, *72*, 041801.
(51) Narayanan, B.; Pryamitsyn, V. A.; Ganesan, V. *Macromolecules* **2004**, *37*, 10180.
(52) Fleer, G. J.; Cohen Stuart, M. A.; Scheutjens, J. M. H. M.; Cosgrove, T.; Vincent, B. *Polymers at Interfaces*; Chapman and Hall: London, 1993.
(53) Papadakis, C. M.; Almdal, K.; Mortensen, K.; Posselt, D. *J. Phys. II* **1997**, *7*, 1829.
(54) Fredrickson, G. H.; Helfand, E. *J. Chem. Phys.* **1987**, *87*, 697.
(55) Onuki, A. *Phase Transition Dynamics*; Cambridge University Press: Cambridge, 2002.
(56) Morozov, A. N.; Zvelindovsky, A. V.; Fraaije, J. G. E. M. *Phys. Rev. E* **2000**, *61*, 4125.

MA0708850